NATIONAL AERONAUTICS AND SPACE ADMINISTRATION

Ranger VII
Photographs of the Moon
Part I: Camera "A" Series

PHOTOGRAPHIC EDITION

JET PROPULSION LABORATORY
CALIFORNIA INSTITUTE OF TECHNOLOGY
August 27, 1964

NATIONAL AERONAUTICS AND SPACE ADMINISTRATION

Ranger VII
Photographs of the Moon
Part I: Camera "A" Series

PHOTOGRAPHIC EDITION

JET PROPULSION LABORATORY
CALIFORNIA INSTITUTE OF TECHNOLOGY
August 27, 1964

Jet Propulsion Laboratory
California Institute of Technology

Prepared under Contract No. NAS 7-100
National Aeronautics and Space Administration

Ranger VII Photographs of the Moon
Part I: Camera "A" Series

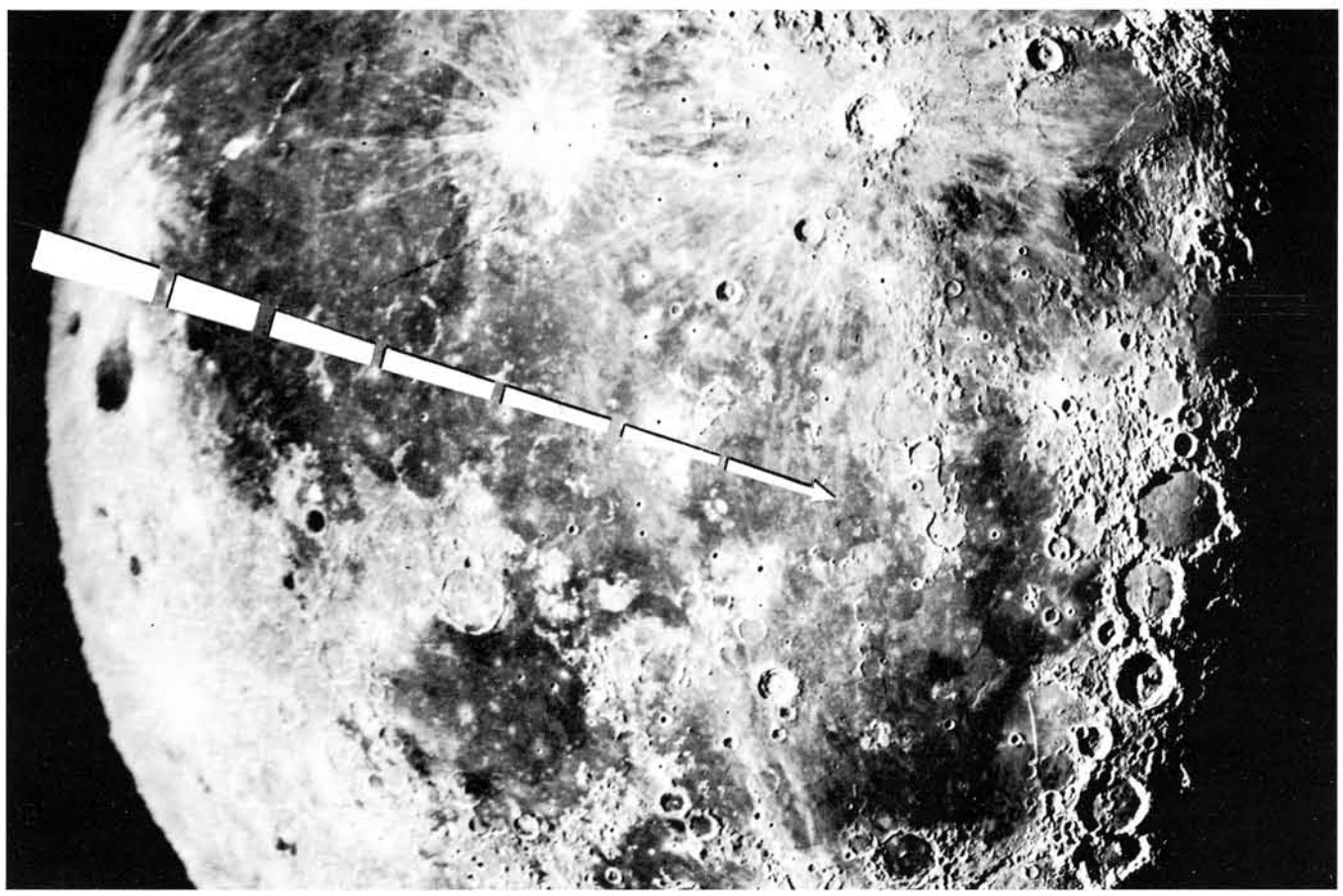

View of impact area under illumination conditions encountered by *Ranger VII

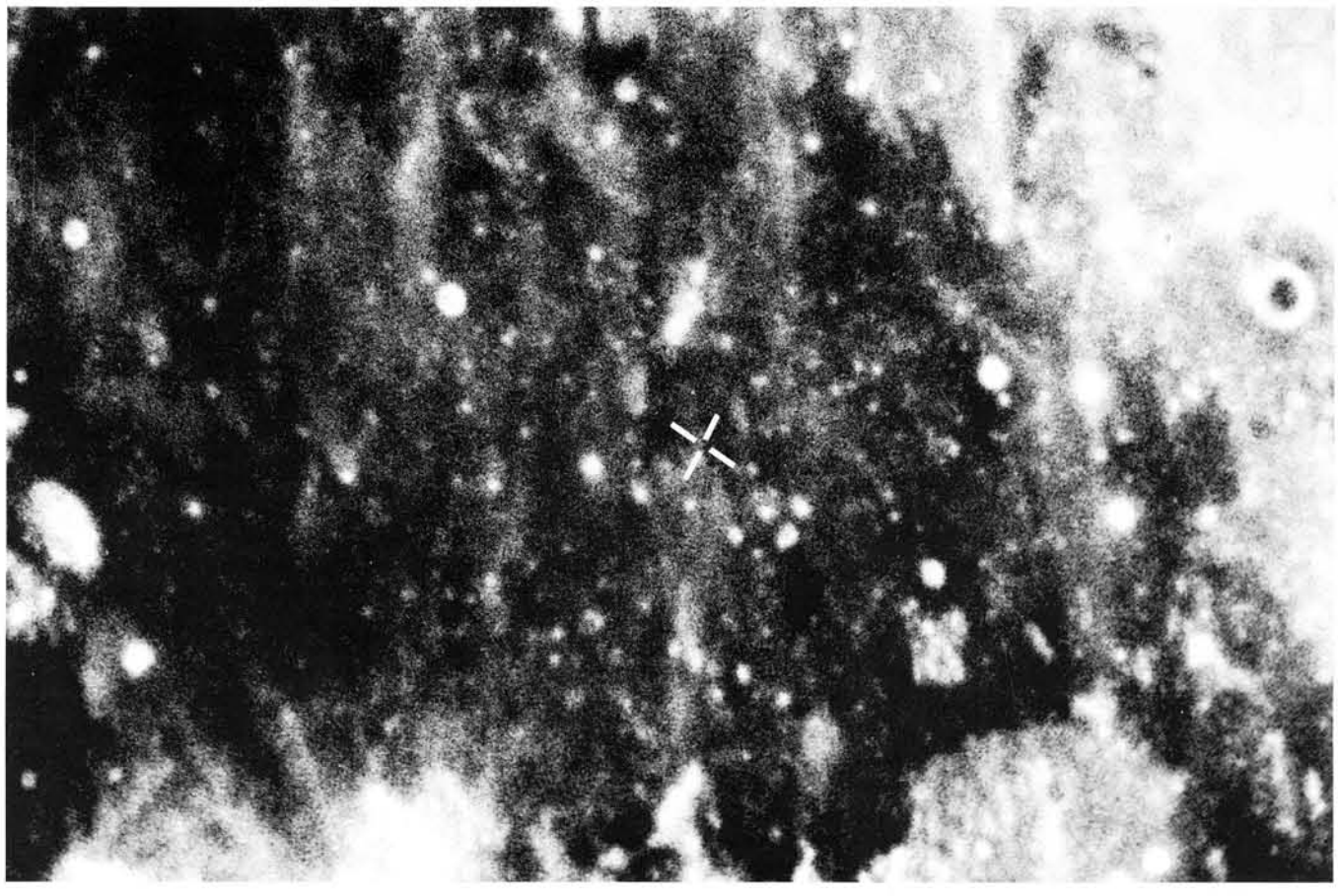

Enlarged view of impact area under full-Moon illumination*

* *Photographs courtesy Lunar and Planetary Laboratory, University of Arizona, Tucson, Arizona*

PREFACE

The *Ranger VII* mission terminated with the acquisition of some 4000 television records of a preselected area of the lunar surface. Included in this atlas, the first collection of the records, is the complete set of photographs taken by the widest-angle camera—the A camera series. The signals from six television cameras aboard the spacecraft were transmitted during the last 17 min of flight. The picture taking spanned a distance range from slightly more than a lunar radius to approximately 480 meters above the surface.

The mission objective of *Ranger VII,* to obtain closeup pictures of the lunar surface which would be of benefit to both the scientific program and the manned program, was carried out flawlessly. Impact occurred 31 July 1964, at 13:25:49 GMT, and the six cameras, two wide-angle and four narrow-angle, carried out their assigned tasks. The A camera, having an f/1 lens of 25-mm focal length and a vidicon target area of 11×11 mm, had a field of $25 \times 25°$. The B camera, with an f/2 lens of 38-mm aperture and 76-mm focal length, and a detector of the same dimension as the A camera, had a field of $8.4 \times 8.4°$. Two of the P cameras utilized lenses identical to that of the A camera, and two were identical to the lenses used in the B camera. The size of the detector plate in the P camera was 2.8×2.8 mm. The density of the scan lines was the same in all cameras, being about 0.010 mm on the detector plate. This fine grid caused the TV pictures to have essentially the quality of photographs.

As the text following this Preface states in more detail, the trajectory of the spacecraft inclined 25.8° from the normal to the lunar surface at the impact point. The optical axis of the A camera differed 5° from this trajectory near impact so that all A frames contain the impact point and, when viewed in sequence, cause the lunar landscape to open up around this point. The optical axis of the A camera was inclined 25° with respect to the normal. The B camera axis deviated about 8° from the trajectory in the opposite sense, making a 13.5° angle with the direction of the A camera. The B frames, therefore, do not nest and require the A frames for their relative location and identification of features.

The first third of the photographs taken with the 76-mm focal-length cameras appear to match closely the resolution of the best photographs of the Moon previously obtained with Earth-based telescopes. The first two-thirds of the pictures taken with the three 25-mm focal-length cameras have a resolution somewhat inferior to the best Earth-based photography. These early frames are, nevertheless, of scientific interest because (1) they show a new aspect of the Moon and are, therefore, of photogrammetric value, (2) they provide important information of internal positional accuracy and consistency of the records, and (3) they provide photometric controls and other checks on camera and TV performance. The later frames taken by all of the cameras were, of course, far superior to Earth-based photographs.

The Frontispiece shows the projection onto a globe of Earth-based photographs, one having nearly the same illumination as photographed by *Ranger VII,* the other showing a near-full-Moon view of the same area and the approximate point of impact.

The selection of the impact point was, of course, influenced by the desirability of achieving a near-terminator impact in order to obtain shadows and contrast from shallow relief detail. However, camera sensitivity and possible spacecraft inaccuracies restrict the impact point selection to about 15–25° from the terminator. From the standpoint of the lunar manned space flight program, it is desired that the impact area be one of typical mare and near the lunar equator. The selected impact region is a relatively detached mare or sinus between Oceanus Procellarum (upper left) and Mare Nubium (right, toward the terminator), bounded by the Riphaean Mountains on one side and the bright, cratered area containing Guericke and Parry–Bonpland on the other. The mare region is traversed by outlying crater rays of both Copernicus and Tycho. These rays are shown most distinctly at full Moon (see Frontispiece). Since the area is not far from the great circle connecting Copernicus and Tycho, the source of each ray should be carefully considered. It appears that the impact point occurs in the trailing end of a fan-shaped Tycho ray, with another similar ray starting to the northwest. The very bright broken patch above the impact point is a mountain range, prominently shown on the TV records.

The impact region appears to consist primarily of tertiary craters and grooves associated with a prominent group of secondary craters nearby. There seems to be a close correlation between ray intensity and crater density. Some regions largely outside the ray system are also included in the records.

The initial scientific evaluation of the *Ranger VII* records has been assigned to the following scientific investigators:

Principal Investigator	Dr. Gerard P. Kuiper, Director, Lunar and Planetary Laboratory, University of Arizona, Tucson, Arizona
Co-experimenters	Mr. R. L. Heacock, Chief, Lunar and Planetary Instruments Section, Jet Propulsion Laboratory, Pasadena, California
	Dr. E. M. Shoemaker, Chief, Astrogeology Branch, United States Geological Survey, Flagstaff, Arizona
	Dr. H. C. Urey, Professor at Large, School of Science and Engineering, University of California at La Jolla, California
	Mr. E. A. Whitaker, Research Associate, Lunar and Planetary Laboratory, University of Arizona, Tucson, Arizona

The programs initiated to date include the following:

1. Production of planimetric maps and photomosaics
2. Photogrammetry, height measurements
3. Slope measurements, using the available photometric calibrations
4. Image cleanup (analog and computer), enhancement, and image composition
5. Crater analysis and statistics
6. Stratigraphic and surface texture studies

The reproductions in this atlas were made photographically in order to preserve the rich image content of the records. The following steps were involved in the copying process. From the prime negative 35-mm film, a contact positive 35-mm film was produced. This positive was mounted in a specially prepared holder to avoid scratching the film during transport. The holder had a conventional glass lower plate and an upper plate of specially prepared glass to prevent Newton rings. Enlargements of all of the A camera frames were then made onto 8 × 10-in. sheets of Plus-X film, using a special enlarger; this device has the capability of reducing large density gradients over the field without reducing local contrasts. The 199 negatives so produced were then used to make the contact prints which comprise this atlas.

There are some specks and other minor defects in the records that repeat from frame to frame and which are due to the vidicon and recording apparatus. Since the user of this atlas can readily ascertain their location by intercomparison of different frames, no listing of these specks is included. No retouching of any kind has been effected in these records. The pictures are presented with North approximately at the top, in accordance with astronautics convention.

The last *Ranger VII* picture was not taken with the A camera; the final photograph in the A series therefore does not show the highest resolution obtained. The last picture taken by *Ranger VII* before impact was published immediately after the mission among the first photographs released.

The high quality of the data obtained from the *Ranger VII* mission made it feasible to publish this atlas at this early date. It was decided to do so in order to place the photographs in the hands of the scientific community as soon as possible, and for use in the preparation of subsequent lunar missions. The A frames were chosen for first publication because of their large area of coverage and because they contain the impact point.

GERARD P. KUIPER

ACKNOWLEDGEMENTS

The lunar photographs contained in this atlas are one significant result of the National Aeronautics and Space Administration's Lunar and Planetary Programs—specifically the *Ranger* project. This project is being managed for NASA by the Jet Propulsion Laboratory, California Institute of Technology, which is directed by Dr. W. H. Pickering.

The *Ranger* team includes members from several of the NASA centers, numerous industrial concerns, universities, and other Government agencies. The many elements of the team are widely dispersed throughout the United States, and additionally include tracking stations at Johannesburg, South Africa, and Woomera, Australia, operated by the respective governments of these countries.

The *Ranger VII* mission was a classic "textbook" operation. The precision with which it was executed and the high quality of the results are due to the excellent and dedicated manner in which each member of the team did his job. To name all of the organizations and individuals contributing to the project is, regrettably, an impossible task. However, the man responsible for guiding their efforts toward a single purpose, Mr. H. M. Schurmeier, the JPL *Ranger* Project Manager, should be mentioned.

In addition to the organizations and people referred to above who were directly involved in the mission, credit is due to a number of individuals who made significant contributions during the early years of the project and have since moved on to other tasks.

NASA is indebted, as will be the many scientists and engineers who will use these pictures, to each member of this team. To them goes the credit for the outstanding success that has been achieved. It is, therefore, to all of the participants in the *Ranger* project, both past and present, that this atlas is dedicated.

HOMER E. NEWELL

Associate Administrator for
Space Science and Applications

National Aeronautics and
Space Administration

CONTENTS

TABLES

FIGURES

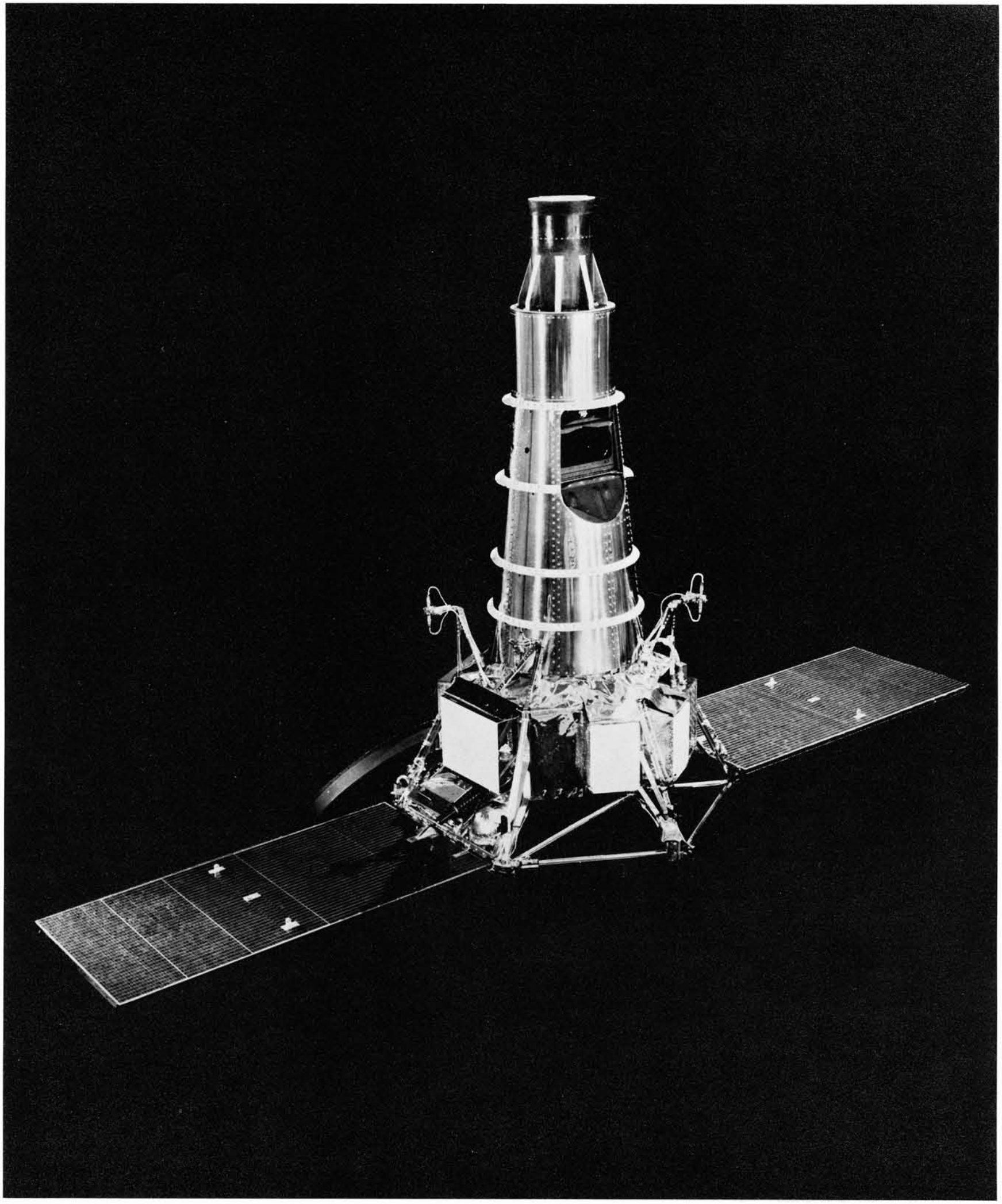

I. INTRODUCTION*

The development of the basic *Ranger* spacecraft system was initiated in 1959. The spacecraft was conceived as a fully attitude-stabilized platform from which lunar or planetary observations could be made by mounting alternate payloads on top of the basic spacecraft. A new concept involving a parking orbit was also proposed in order to permit maximum payloads to be injected on the most efficient lunar or planetary trajectory. The technique involves two burns of the second stage of the *Atlas/Agena B* launch vehicle to compensate for the nonideal geographical location of the launch pad and provide a more practical daily launch window.

The advantages to be gained from an attitude-stabilized spacecraft configuration include:

1. Maximum effectiveness in generating power by accurately pointing solar panels at the Sun.

2. Establishment of an accurate angle-reference system for use as a coordinate system in which to perform a midcourse maneuver to trim the flight path and as a reference for terminal orientation.

3. Provision of maximum communications by accurately pointing a high-gain antenna at the Earth.

4. Feasibility of using scientific instruments which require direction determination and/or control to make their observations.

The nominal sequence of spacecraft operation after separation from the *Agena B* involves extending the solar panels and pointing the roll axis at the Sun for maximum solar power. The attitude-control system uses inputs from optical sensors to control small cold-gas jets to obtain and maintain proper attitude orientation. When the spacecraft is sufficiently far from the Earth, the antenna hinge angle is nominally set to point the optical Earth sensor and the high-gain antenna at the Earth. The control jets roll the spacecraft until the optical Earth sensor locks onto the Earth and high-gain directional communication is made possible. Establishing Sun and Earth orientation in this manner provides full attitude stabilization for the cruise mode.

The midcourse maneuver is performed by establishing an appropriate pointing direction relative to the Sun–spacecraft–Earth coordinate system and firing a midcourse rocket engine to obtain the desired velocity increment. A radio-command system transmits the angles and velocity-increment requirements to the spacecraft. The commands are stored and acted upon in a controlled sequence using a gyro-stabilized reference system to achieve the required orientation. Once the midcourse maneuver is complete, the spacecraft automatically resumes the cruise-mode orientation.

The spacecraft has the ability to perform a limited angular orientation in a terminal-maneuver sequence if required. The principal constraint upon orientation geometry involves maintaining the high-gain antenna pointed at the Earth.

The *Ranger* Block III project (consisting of *Rangers VI* through *IX*) was initiated in mid-1961. The objective of high-resolution photographs of the lunar surface could conceptually be achieved through any of several approaches, ranging from systems using long focal-length optics to a technique involving a retro firing sequence. The approach which was selected used more conventional techniques and available technology. A high-power transmitter was used to provide sufficient video bandwidth for a rapid framing sequence of television pictures to impact. Two separate channels were proposed for redundancy and to permit both narrow- and wide-angle camera coverage.

The camera fields of view were arranged to provide overlapping coverage so that, with a nominal terminal orientation, a nesting sequence of photographs would be obtained from at least one of the wide-angle cameras. The narrow-angle camera frame sequence is over ten times faster than the wide-angle camera sequence to permit operation closer to the surface for higher resolution. The final design of the system included two cameras in the wide-angle system and four cameras in the narrow-angle system.

*The sections that follow were prepared by Gerald M. Smith, Donald E. Willingham and William E. Kirhofer of the Jet Propulsion Laboratory, California Institute of Technology.

II. *RANGER VII* MISSION DESCRIPTION AND TRAJECTORY

Ranger VII was launched from Cape Kennedy on July 28, 1964, at 16:50:08 GMT, after a very smooth countdown with no unscheduled holds. The launch resulted in a trajectory which would impact the far side of the Moon. The necessary midcourse maneuver was then calculated and executed to impact the desired target area. During the launch, all booster-vehicle and spacecraft events occurred as planned. The initial boost placed the *Agena B* and spacecraft in a parking orbit over the Atlantic Ocean, where the *Agena B* second burn was initiated. Termination of this boost phase accomplished the injection of the spacecraft into an Earth–Moon transfer orbit. After separation from the *Agena*, the spacecraft solar panels were extended and Sun and Earth acquisition were accomplished in a normal manner.

Telemetry and doppler velocity data received following the midcourse-motor burn confirmed the desired midcourse correction. The spacecraft then returned to cruise mode by reacquiring the Sun and Earth. Post-midcourse tracking data indicated that the spacecraft would impact the Moon in the target area, 11°South and 21°West selenocentric coordinates.

After the midcourse maneuver, the terminal approach was analyzed considering the angle of illumination of the lunar surface, the direction of the velocity vector of the spacecraft, and the pointing direction of the camera system. It was established that no terminal maneuver was required for the photographic sequence. The wide-angle camera system started taking pictures at 13:08:36 GMT on July 31, 1964, 17 min, 13 sec prior to impact. The narrow-angle system initiated transmission of pictures at 13:12:09 GMT, 13 min, 40 sec prior to impact. Both camera systems operated to impact at 13:25:49 GMT. The last narrow-angle picture was taken at 0.18 sec before impact from an altitude of approximately 480 meters. The area read out covers approximately 30 × 50 meters and has a surface resolution of about 0.5 meters.

The spacecraft encountered the Moon in direct motion along a hyperbolic trajectory, with incoming asymptote direction at an angle of − 5.57° from the lunar equator. The orbit plane was inclined 26.84° to the lunar equator. Thus, the subspacecraft trace on the lunar surface was initially above the lunar equator by approximately 5° and proceeded in a southeasterly direction, crossing the equator at a selenocentric west longitude of 42.2° in a direction 28.6° south of east some 46 min prior to impact.

At the time of the first wide-angle picture, the spacecraft selenocentric south latitude and west longitude were 3.3 and 35.9°, respectively. At impact, the velocity vector was 25.8° from the local vertical in a direction, projected into the local horizon, 114.9° east of north. The velocity of the spacecraft at impact was 2.62 km/sec. The encounter geometry illustrated in Fig. 1 relates the trajectory and lunar trace with the lunar area viewed by each wide-angle camera. In addition, Fig. 1 gives the trace on the lunar surface viewed by the optical axis of the wide-angle cameras prior to lunar impact.

During the cruise mode and terminal portion of flight, the *Ranger VII* spacecraft was stabilized by a cold-gas jet attitude-control system. This system derived its reference from the Sun and Earth. The Sun sensors allowed the spacecraft roll axis to be aligned with the −Z axis toward the Sun. The Earth sensor was used to orient the high-gain antenna toward Earth. This orientation kept the Earth in the −Y,Z plane of the spacecraft. The X, Y, and Z orthogonal coordinate system associated with the spacecraft is defined in Fig. 2.

The reference direction for the camera alignment was 38° from the Z (or roll) spacecraft axis. The optical centers of all the cameras were within 0.5° of the spacecraft Y,Z plane. The relative camera alignment with spacecraft coordinates is shown in Fig. 3.

At lunar encounter, the Moon was very near its third quarter, with the projection of the Sun at a selenocentric north latitude and west longitude of 0.9 and 87.6°, respectively. The lunar libration was such that the projection of the Earth was at a lunar north latitude of 5.8° and west longitude of 5.2°. Thus, with the Sun and Earth as reference, the Y,Z spacecraft plane was then inclined to the lunar equator by approximately 5°. Because the camera axes are nearly contained in the Y,Z spacecraft plane, the cameras were, in general, pointing south of the lunar equatorial plane by approximately 5°. This explains the southerly position from the trajectory trace of the area viewed by the optical centers as illustrated in Fig. 1.

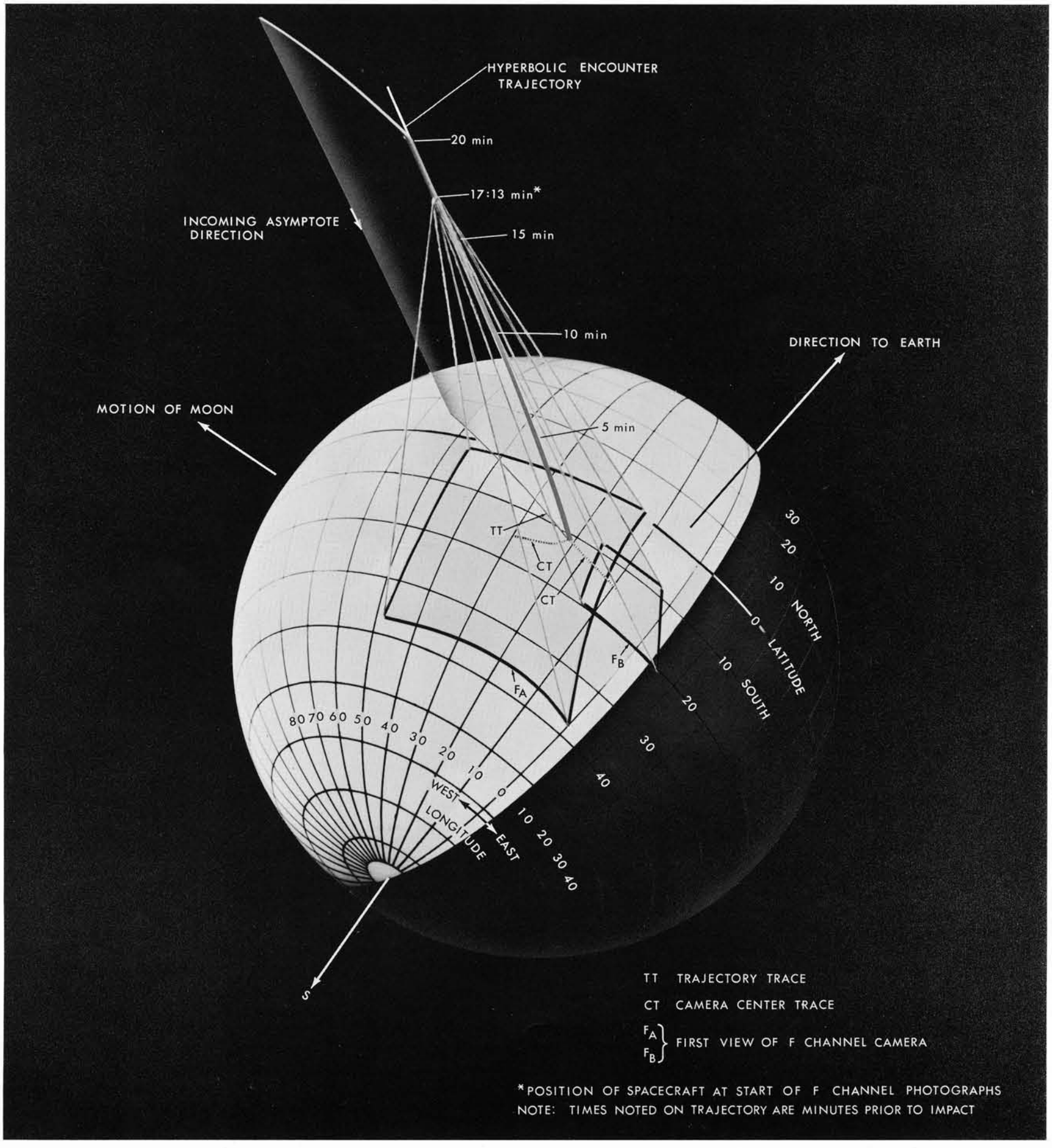

Fig 1. Lunar encounter geometry

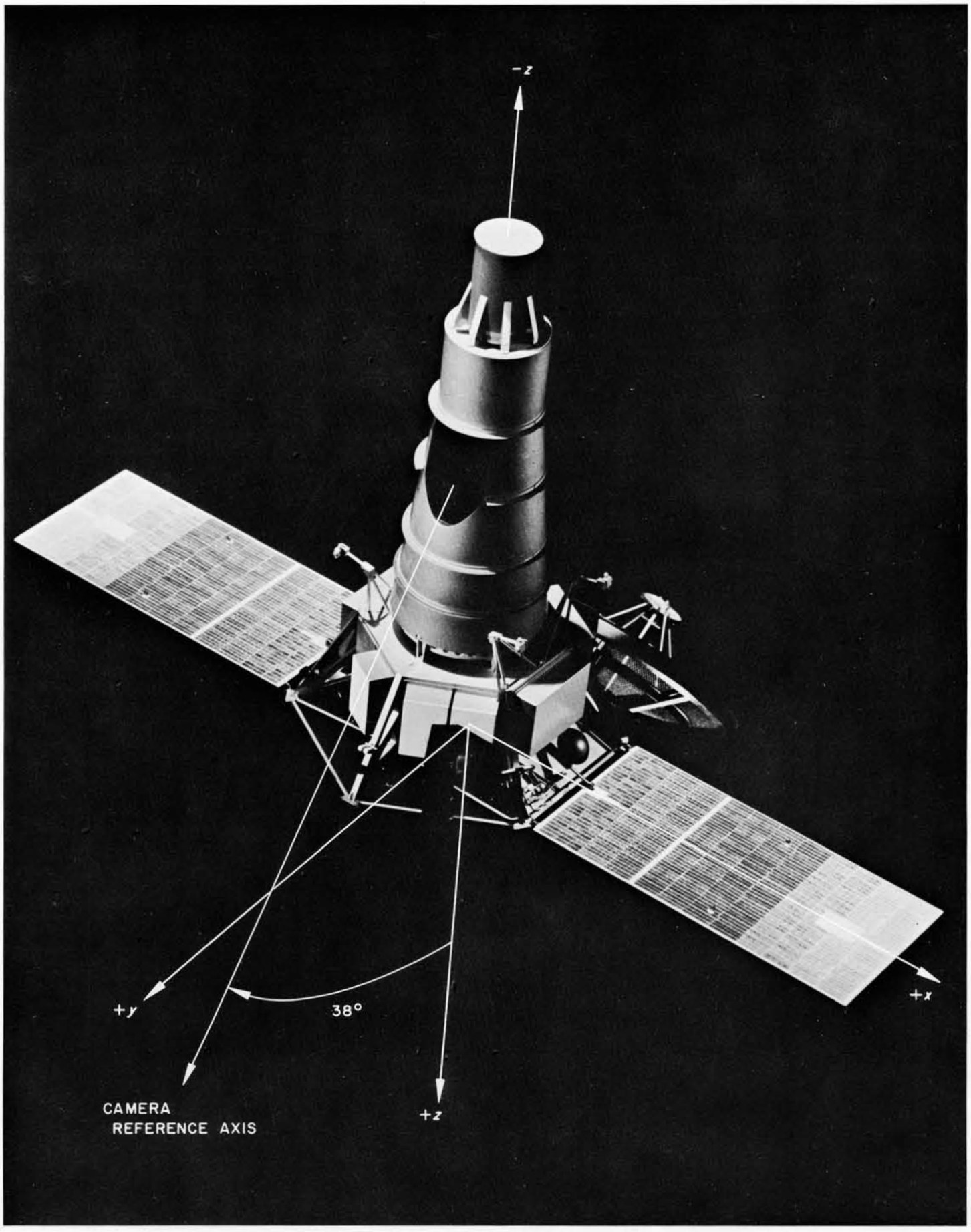

Fig. 2. Spacecraft coordinate system

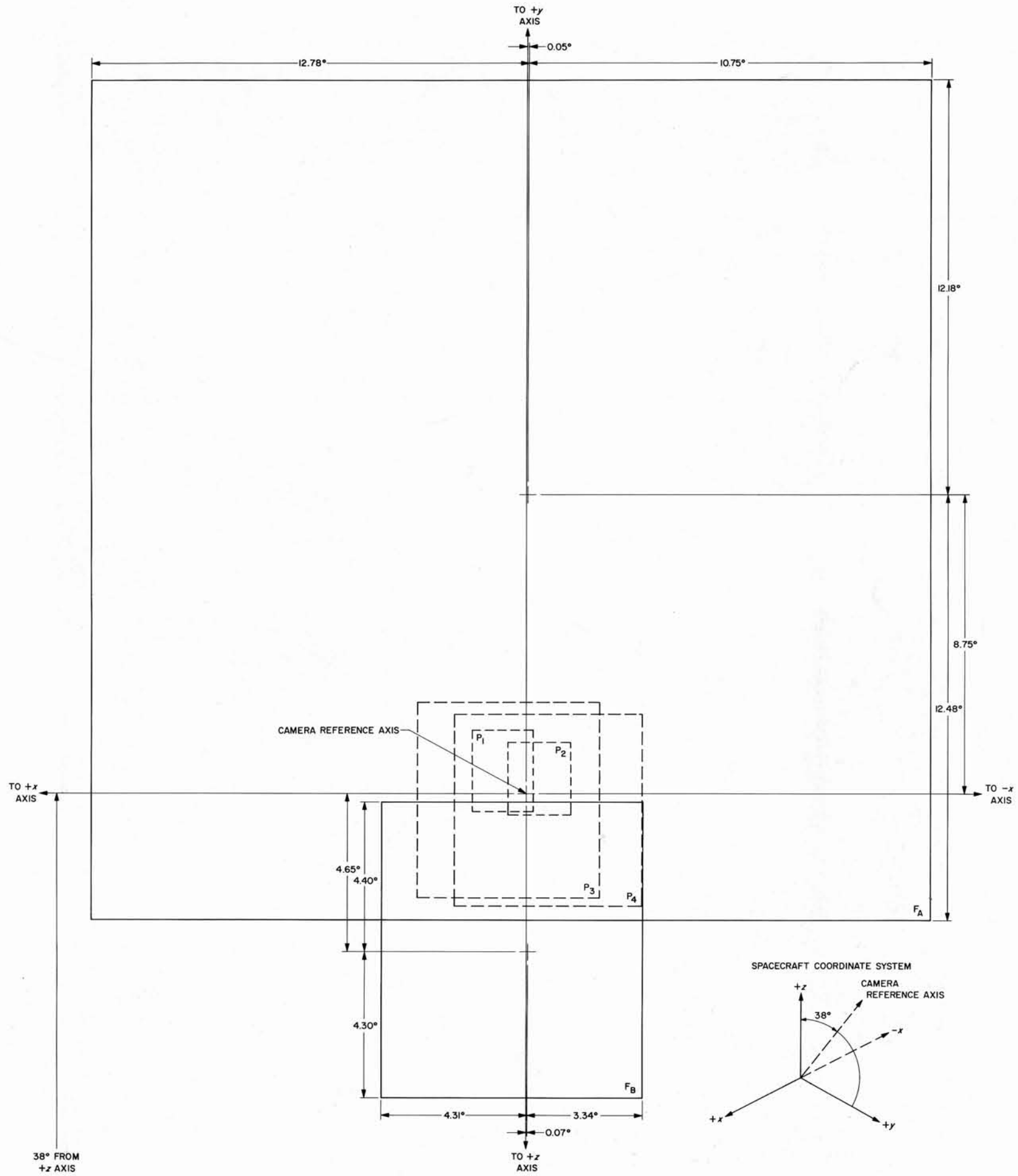

Fig. 3. *Ranger VII* camera fields of view (a) Cameras A and B

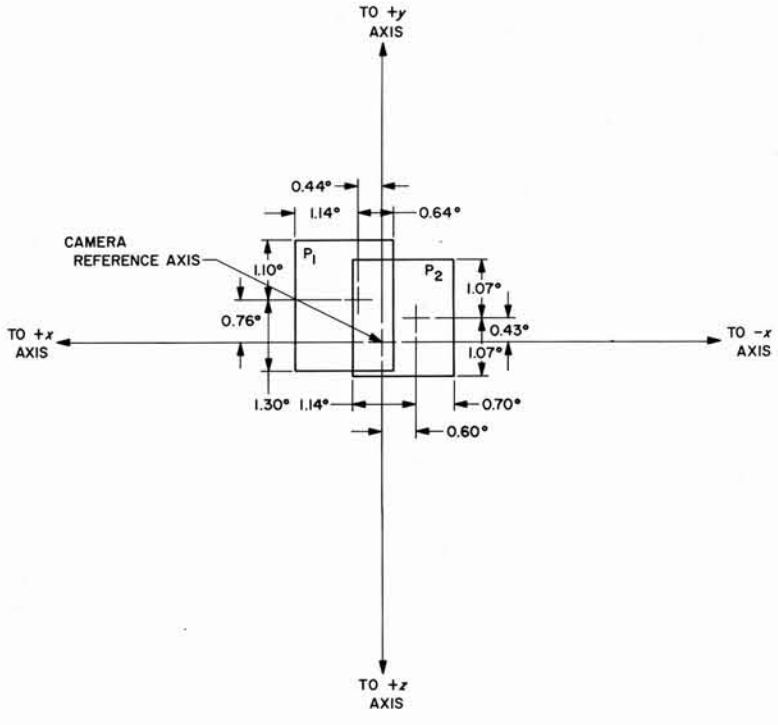

(b) Cameras P_1 and P_2

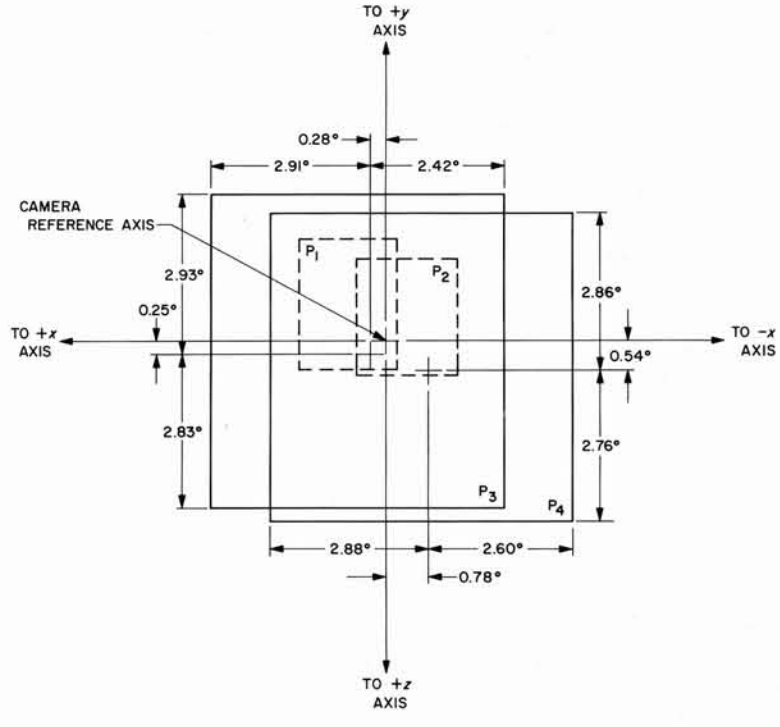

(c) Cameras P_3 and P_4

Fig. 3. (cont'd)

III. IMPACT-AREA SELECTION AND CAMERA TERMINAL ALIGNMENT

The selection of optimum lunar aiming areas for the *Ranger* spacecraft requires consideration of lunar topography and photometry, camera characteristics, and spacecraft viewing geometry and trajectories. In addition, possible nonstandard flights (in terms of that desired) offer an infinite number of situations from which the optimum mode of operation must be selected. A quantitative method for quickly arriving at such decisions prior to and during flight is thus a necessity. For this purpose, a mathematical model utilizing a complete camera systems description, a generalized lunar photometric function, a human observer model, and a spacecraft-trajectory description has been developed and programmed into a digital computer (Refs. 1 and 2). Because of simplifying mathematical assumptions and lack of experimental verification prior to the *Ranger VII* flight, the output of the computer program is considered only a relative indication of system performance. This performance indicator, denoted as the "figure of merit," is an estimate of the smallest surface feature that can be detected by an observer viewing the output 35-mm film positive from the camera system. More explicitly, the figure of merit is defined as the size of the smallest square element on the lunar surface having representative contrast with the background which can be detected by an observer viewing the 35-mm film.

To specify the contrast of the square surface element and the general surface luminance distribution, one must have knowledge of the lunar photometric properties. In deriving a generalized photometric function, mare observations were selected from the work of Sytinskaya and Sharonov (Ref. 3). These observations were combined and averaged to obtain a generalized reflectivity model as a function of two angles—phase angle and luminance longitude (Ref. 4). With the assumption of photometric uniformity for all levels of resolution and the use of an appropriate solar constant, a prediction of average mare brightness as a function of the above two parameters can be made.

Given the surface photometric characteristics and viewing geometry, the appropriate contrast to be used for calculating the figure of

merit would be that obtained in an average over the most probable surface orientations of lunar relief. For mathematical simplicity, an inverted right-circular cone of given base angle (a computer-program input variable) has been chosen as a representative surface feature. The viewing geometry is, of course, dependent upon the position of the lunar impact area with respect to the terminator, the trajectory characteristics, and the terminal mode orientation of the spacecraft. Hence, the average contrast is strongly dependent upon the position of the point on the lunar surface at which it is calculated.

The 35-mm film transmission distribution produced by the passage of the scene luminance distribution through the camera system can be calculated by use of conventional Fourier-transform techniques. Complete system description requires only the specification of the light-transfer characteristic from scene luminance to output film transmission and the system vertical and horizontal (perpendicular and parallel to the line scan, respectively) spatial sine-wave response functions. By neglecting phase shift, the spatial sine-wave response functions can be approximated by gaussian curves so that each can be specified completely by a gaussian width parameter. The width parameters and light-transfer characteristic of each camera are derived from preflight system calibration. Thus, with the specification of the viewing geometry, the output signal on the 35-mm film can be computed solely as a function of the square surface-element dimension.

The next step is for the human observer to view and interpret the resultant film image. He will, of course, see a certain amount of system noise contributed primarily by system electronics and film granularity. The root-mean-square noise amplitude as a function of film transmission can be determined experimentally with a microdensitometer. It has been assumed that the human observer optimizes viewing conditions and makes the image stand out from the background noise as much as possible. Mathematically, the observer is represented as an optimum filter maximizing the image signal-to-background-noise ratio. The characteristics of this optimum filter are completely determined by the film transmission signal, which, in turn, was created by the luminance distribution from the surface element. Hence, the resultant signal-to-noise ratio is dependent only upon the size of the square surface element being viewed. Therefore, specification of the threshold signal-to-noise ratio required for detection (with a given probability) determines the size of the minimum detectable surface element or figure of merit.

Thus, the figure of merit is a measure of the smallest objects detectable in the scene being viewed, incorporating the effects of the environment in which the system must operate, the nature of the scene, the system's inherent parameters, and the human observer capabilities.

During a preflight operational mode, necessary system parameters and encounter geometry are known. With the assumption of a time before impact at which the last picture is taken and the specification of a representative cone base angle, threshold signal-to-noise ratio, and spacecraft terminal-mode orientation, the figure of merit can be

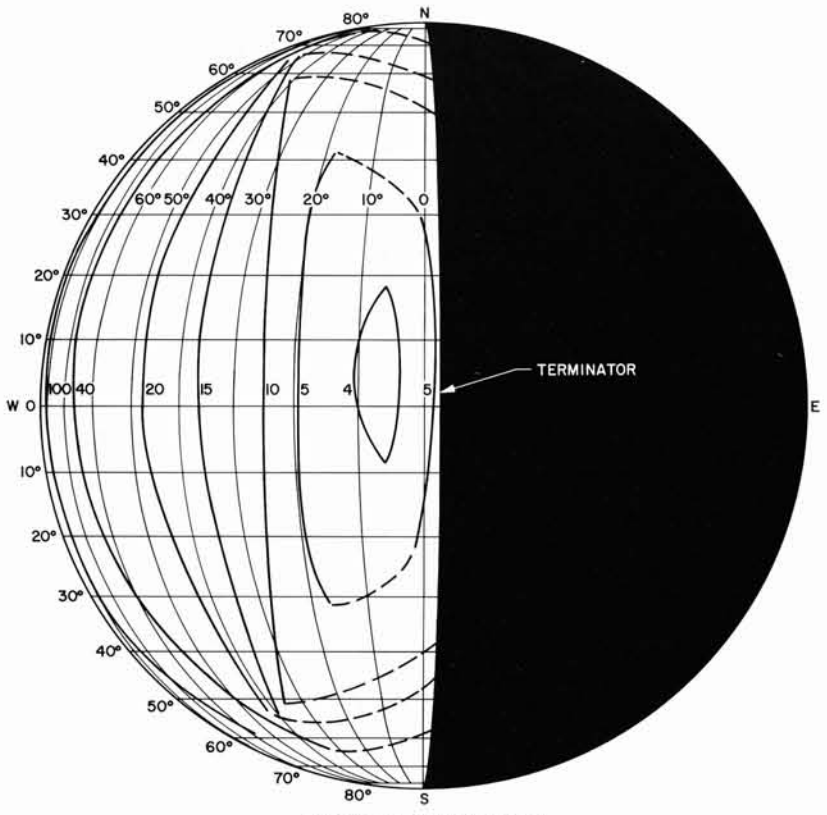

NOTE: NO TERMINAL MANEUVER, 30° BASE ANGLE FEATURE, FRAME TIME 3.84 sec BEFORE IMPACT, *S/N* RATIO = 3.0

FIGURE OF MERIT CONTOURS GIVEN IN METERS

Fig. 4. *Ranger VII* preflight analysis, camera A figure of merit contours

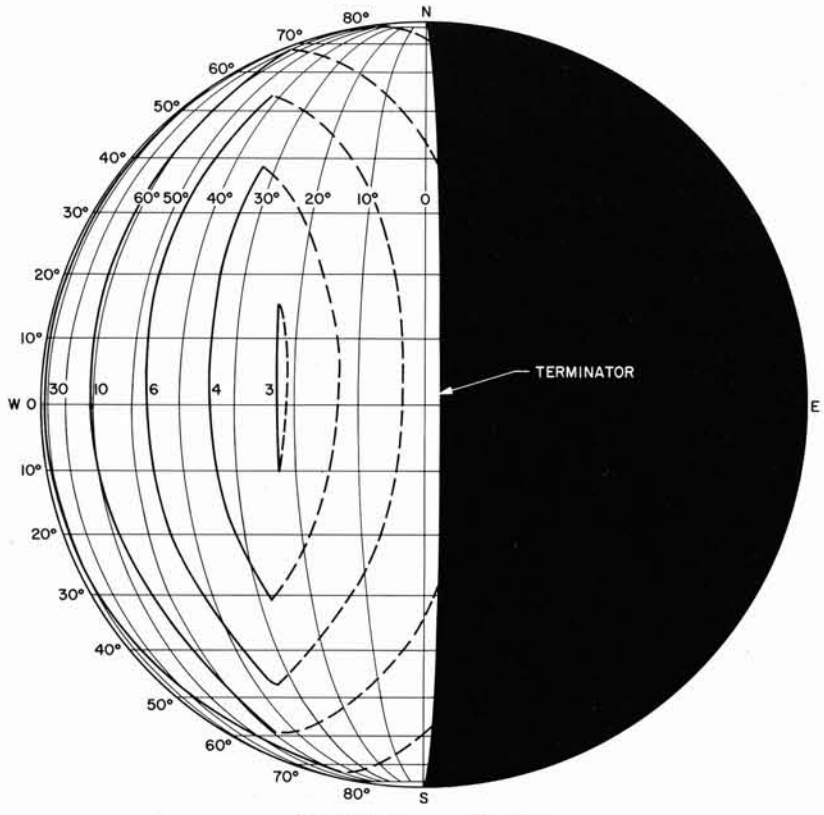

NOTE: NO TERMINAL MANEUVER, 30° BASE ANGLE FEATURE, FRAME TIME 3.84 sec BEFORE IMPACT, *S/N* RATIO = 3.0

FIGURE OF MERIT CONTOURS GIVEN IN METERS

Fig. 5. *Ranger VII* preflight analysis, camera B figure of merit contours

calculated as a function of impact latitude and longitude. In addition, the root-mean-square image motion over the camera field of view is calculated for each impact point. Combined contours are then drawn using only the larger of the two values (figure of merit or image motion); where image motion is the larger, the contours are dashed. In practice, two terminal orientations are examined prior to launch: (1) the normal orientation of the central camera reference axis along the trajectory vector, thus minimizing image motion, and (2) the no-terminal-maneuver orientation.

Representative contours are shown in Figs. 4 and 5. It will be noted that the optimum impact area for camera F_B—that is, the contour which indicates the smallest figure-of-merit value—occurs approximately 25° from the terminator, while for camera F_A, the optimum is about 10° from the terminator. Note also the computer-program input parameters indicated on the Figures.

The contours were further superimposed with lunar topographic characteristics (mare impact areas were desired) and predicted mission aiming accuracies to obtain a primary target area of 11°South latitude and 21°West longitude for a July 28 launch. Primary aiming points were selected for the other possible launch dates in the same manner.

After the *Ranger VII* spacecraft successful launch, injection, and midcourse correction had assured impact in the prelaunch aiming area, the detailed terminal-mode study was begun. In all, seven terminal orientations were examined. The small amount of image motion (0.7 meter in the last P camera frame) and the very desirable surface trace in the no-terminal-maneuver case, combined with the relative insensitivity of the figure of merit to orientation changes within those considered, made the no-terminal-maneuver orientation nearly optimum.

IV. TELEVISION SYSTEM DESCRIPTION

A. Cameras

The *Ranger* Block III spacecraft television system contains six cameras, divided into two separate channels designated P and F. Each channel is self-contained, with separate power supplies, timers, and transmitters. All six cameras are fundamentally the same, with differences in exposure times, fields of view, lenses, and scan rates distinguishing the individual cameras (Table 1).

Table 1. Camera characteristics

Characteristic	Camera					
	A	B	P_1	P_2	P_3	P_4
Focal length, mm	25	76	76	76	25	25
f number	1.0	2.0	2.0	2.0	1.0	1.0
Frame time, sec	2.56	2.56	0.2	0.2	0.2	0.2
Horizontal frequency, cps	450	450	1500	1500	1500	1500
Exposure time, msec	5	5	2	2	2	2
Field of view*, deg	25	8.4	2.1	2.1	6.3	6.3
Target size, mm	11	11	2.8	2.8	2.8	2.8
Scan lines	1150	1150	300	300	300	300
Time between frames, sec	5.12	5.12	0.84	0.84	0.84	0.84

*The actual field of view is somewhat smaller than the given numbers because of the presence of a mask at the edge of the vidicon target which is used to determine scene black on each scan of the electron beam.

One-inch-diameter vidicons are used for image sensing. Electromagnetically driven slit-type shutters expose the vidicons. The image is focused on the vidicon target through the shutter, which is placed slightly in front of the focal plane. The vidicon target is made up of a layer of photoconductive material, initially charged by scanning with an electron beam. The image formed on the photoconductive surface causes variations in resistance across the surface which are a function of the image brightness. These variations allow a redistribution of the charge which remains after exposure. In the *Ranger* cameras, the charge pattern formed by the image on the photoconductor remains much longer than in commercial systems, so that the pictures may be taken more slowly. By slowing down the picture-taking rate, it is possible to use a narrow electrical bandwidth, which simplifies the communications problem in transmission of the signal to Earth. After the image has been formed on the photoconductor by operation of the shutter, an electron beam scans the surface and recharges the photoconductor. The variation in charge current is the video signal, which is then amplified several thousand times and sent to the transmitter, where the amplitude variations are converted to frequency variations. The frequency-modulated signal is amplified, and the signals from the two channels are combined and transmitted to Earth through the spacecraft high-gain antenna.

1. F Channel

The F channel has two cameras — the A camera with a 25° field and the B camera with an 8.4° field. Both have 5-msec exposure times; however, the A camera has a 25-mm f/1.0 lens, while the B camera f/2.0 lens is 76 mm. The combined useful operating range of the two cameras is from about 10 to 2500-ft lambert* scene brightness. This large dynamic range allows for the possibility of the spacecraft impacting in a region with poor lighting conditions without appreciable reduction in the quality of the photographs. The electron beam scans an area approximately 11 mm square in 2.5 sec with 1150 lines. The two cameras operate in sequence, so that only one camera is being scanned at a particular time. This allows the signals from the two cameras to be transmitted over a single transmitter. Since each camera requires 2.5 sec to be scanned and then must wait 2.5 sec while the other camera is scanned, there are intervals of about 5 sec between consecutive pictures on a particular camera. During the waiting period, the cameras erase the residual image from the preceding picture and the shutter exposes the vidicon for the next cycle of operation.

2. P Channel

The P channel contains four cameras, designated P_1 through P_4. The same combination of lens types as in the F channel are used in the P cameras. P_1 and P_2 use 76-mm f/2.0 lenses, and P_3 and P_4 use 25-mm f/1.0 lenses, so that the P cameras have the same dynamic range capability as the F cameras. The primary difference between the two sets of cameras is in the scan rates and the portion of the photoconductive target used. The P cameras scan only a 2.8-mm-square segment of the target with 300 scan lines. The time required to scan the area is 0.2 sec. Again, as with the F cameras, only one camera is being scanned at a time, so that all four are coupled into a single transmitter. The time between consecutive pictures on a particular camera is 0.84 sec. Because of the smaller target area of the P cameras, the field of view is correspondingly smaller than that of the F cameras. P_1 and P_2 have approximately 2.1° fields, while the P_3 and P_4 fields are approximately 6.3°. In addition to the differences described above, the P camera exposure times are shorter than the F exposures. The P shutters are set for a 2-msec exposure to reduce image motion as the spacecraft approaches the lunar surface. The last complete F camera picture is taken between 2.5 and 5 sec before impact, while the last complete P camera picture is taken between 0.2 and 0.4 sec because of the faster cycling rate on the P cameras. Image motion is therefore more severe in the last P camera pictures, and shorter exposure times are required. The sequence for one cycle of operation of the P cameras is P_1–P_3–P_2–P_4, so that photographs are taken alternately by a 76-mm lens and a 25-mm lens.

B. Receiving and Recording Equipment

The television signals from the spacecraft are received with 85-ft-diameter antennas at two sites, located about 10 mi apart at Goldstone, California. The signals are amplified and mixed by a local oscillator to reduce the signal center frequency to 30 Mc and then sent to the television receiver. Another mixing operation reduces the

*1 ft lambert = 1.0764×10^{-3} lamberts

frequency to 4.5 and 5.5 Mc, respectively, for the two channels. The signal frequency variations are then converted back to amplitude variations in two demodulators (one for each camera channel), whose outputs are the same as the video signals originally generated in the cameras. The video signals are used to control the intensity of an electron beam in a cathode-ray tube, which is scanned in unison with the electron beam in the cameras. The cathode-ray tube reconstructs the original image, which is then photographed on 35-mm film. These recording devices are similar to the commercial kinescopes used for recording television programs on film. Again, there is one recording device for each camera channel, so that two pictures are being recorded at any instant in time, one F camera and one P camera. All the functions discussed above are duplicated at both receiving sites, with one exception. One site utilizes a single film recorder to record the four P cameras, while the other site maintains two film recorders and records both camera channels.

In addition to the film recorders, another means of recording the data is used. The 4.5- and 5.5-Mc signals that go to the demodulators are also sent to another mixer, which reduces the center frequency still further to 500 kc. These signals are recorded on magnetic tape at both sites. Two such recorders are used at each receiving station. In order to obtain film records from the magnetic tapes, they are played through a demodulator, and the video signal is applied to the film recorder as discussed above.

C. *Camera Calibration*

The calibration of the cameras involves three principal aspects of camera performance: light-transfer characteristic (photometric calibration), sine-wave response (modulation transfer function), and system noise. In addition, data on geometric distortion are obtained.

1. Light-Transfer Characteristic

In order to obtain some absolute photometric information about the lunar surface, camera sensitivity is measured as a function of scene brightness. Using a set of collimators to simulate the scene, the cameras are exposed to various brightness levels before launch, and the camera signal output is recorded on magnetic tape. The magnetic tape is then played back through the recording equipment at Goldstone, and the calibration data are recorded on the same film as the lunar photographs in order to eliminate errors due to differences in film strips processed at different times. The variation in development of a single strip from one end to the other is negligible. The net result, then, is the functional relationship between film density and collimator brightness. In order to account for the differences between the spectral emission characteristics of the collimators and the reflected solar radiation from the lunar scene, a series of spectral measurements is made on all the instrumentation. A correction factor is then calculated to correct the collimator brightness to lunar scene brightness. Reference 5 describes this procedure. Since the photometric calibration is on the same film as the photographic data, it can be carried through subsequent copying operations. A typical light-transfer characteristic of scene brightness vs. negative film density for a 76-mm and a 25-mm camera is shown in Fig. 6. The accuracy of the photometric calibration is limited primarily by vidicon nonuniformities and variations in exposure times, and is expected to be about $\pm 20\%$.

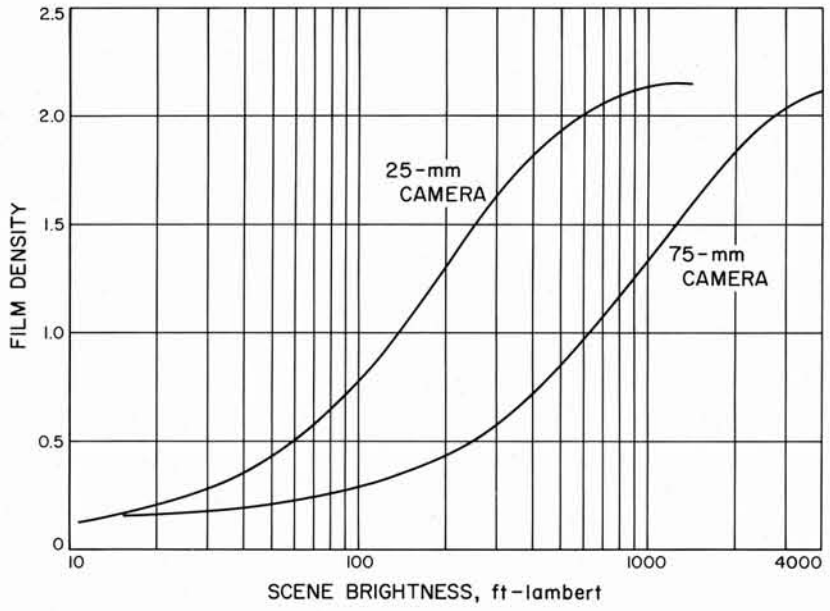

Fig. 6. Typical light-transfer characteristic

2. Sine-Wave Response

In order to obtain the approximate mathematical description of the system required for the figure of merit, it is necessary to determine the sine-wave response of the system. There are a number of ways of obtaining such data. The most direct method is the use of slides with sinusoidal variations in transmission which are then placed in the calibration collimators to illuminate the cameras. A film recording is made, and then the film is scanned with a microphotometer to determine the sine-wave response. A typical response curve is shown in Fig. 7.

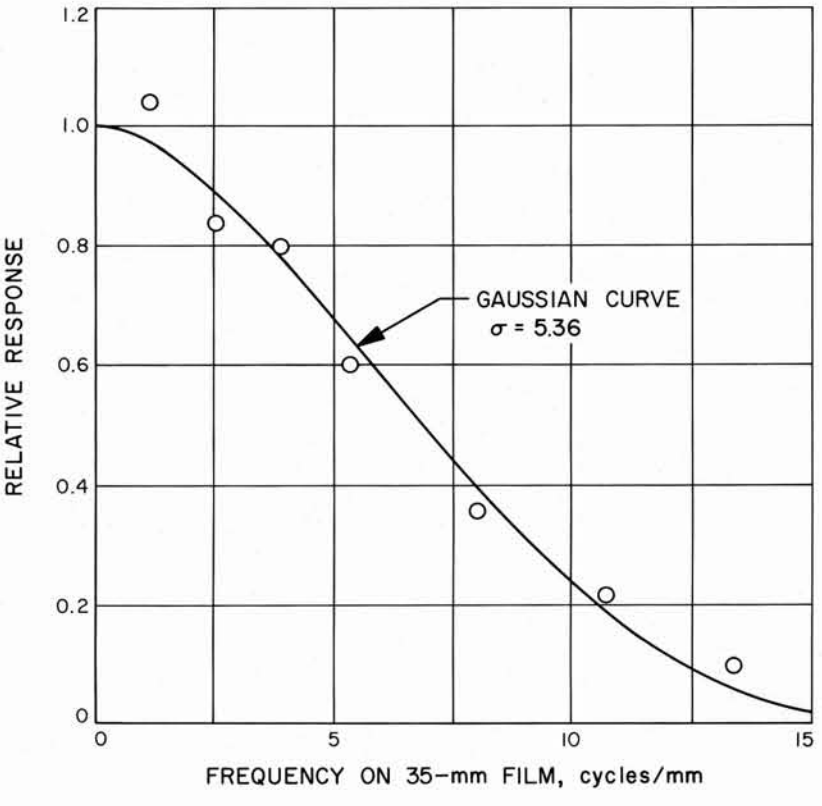

Fig. 7. Typical sine-wave response

3. System Noise and Geometric Distortion

Noise is one of the critical parameters of a photographic system which is required to characterize the system. For a television system, it is convenient to combine film granularity with electrical noise generated in the camera and the communication system to obtain an over-all measure of system noise. The over-all noise is measured by scanning a film recording with a microphotometer. The resulting record is then analyzed to calculate the root-mean-square variations in transmission.

Geometric distortion is determined by inserting a slide in the collimators which has been ruled horizontally and vertically. Photographs of the slide are then used to correct the distortion.

D. Film Recording and Processing

Because of the short time duration of the picture-taking sequence, it is prudent to set up the film recorder brightness levels well in advance of the mission. It is necessary, therefore, to make the dynamic range of the recorder correspond to the dynamic range of the camera system. This precludes the optimum setup for the particular lighting conditions of the impact area; however, no information is lost permanently because the magnetic tape can be played back after the mission, with the film recorder setup optimized.

The optimum density range in the film is determined by several practical characteristics of the film recorder, such as cathode-ray tube brightness, resolution, film camera aperture, and the film itself. An analysis of these parameters indicated that a density range of 1.6 from scene black to scene white was the best choice in terms of minimizing the effects of film granularity.

The film used for the *Ranger VII* mission was Eastman Kodak television recording film, type 5374. The negatives were developed by a commercial film processor to a gamma of 1.4. The processed negatives were then contact printed in a continuous film printer to obtain a master positive. The film used for the positive was Kodak type 5235, a fine-grain panchromatic film. The positive was developed to a gamma of 1.0. The photographs in this atlas were produced from the master positive by making 8 × 10-in. negatives using an electronic dodging device. The negatives were then used to contact print the photographs, with some additional manual dodging in the contact printer.

V. CAMERA A TABLE OF VALUES

The general surface coverage of the *Ranger VII* cameras has been discussed. The nesting and coverage of camera A are shown more definitively by the five photographs of Fig. 8. The reference number of each of these pictures within the entire series of camera A pictures is also given.

Repetition of some permanent camera surface characteristics—that is, the camera fingerprint—will be noted in each frame. These irregularities should be ignored in any photograph interpretation studies.

The parameters listed in the preliminary table of values (Table 2) are defined below:

Spacecraft

Altitude: The distance from the spacecraft to the surface directly below.

Latitude, longitude: The selenocentric position of the point of intersection with the surface of a line connecting the spacecraft and the center of the Moon. This defines the surface point directly below the spacecraft.

Photograph

Central reticle: The principal cross mark on the camera face (Fig. 9).

Latitude, longitude: The surface point in selenocentric coordinates covered by the central reticle.

Slant range: The distance from the spacecraft to the surface point covered by the central reticle (Fig. 10).

Inclination of surface: The angle from the local vertical at the central reticle to the camera direction. A normal view to the surface is then 0° inclination. A spherical surface is assumed.

Scale: The distance from the surface point covered by the central reticle to the surface point covered by the reticle immediately to the left of the central reticle (Fig. 9).

Deviation North: Grid north is defined by the straight line drawn from the central reticle to the middle reticle in the north margin of the photograph. The deviation is the clockwise rotation from grid north to the direction of true North at the central reticle. Note that the lunar meridians as plotted on the camera A photographs exhibit some curvature but may be regarded as straight lines from photographs 166 to 199. Convergence of the meridians is appreciable on all photographs, including those of larger scales, and directions at the central reticles cannot be transferred to the left and right margins without introducing errors as large as 3° (Fig. 9).

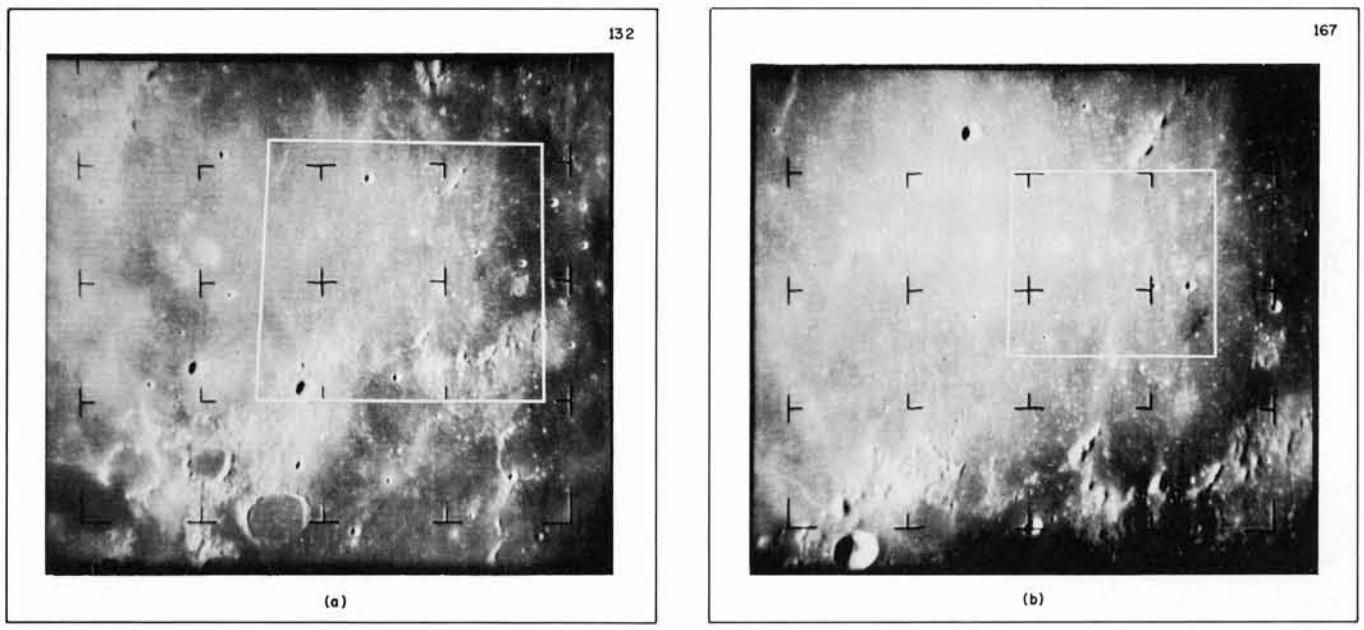

Fig. 8. Camera nesting and coverage

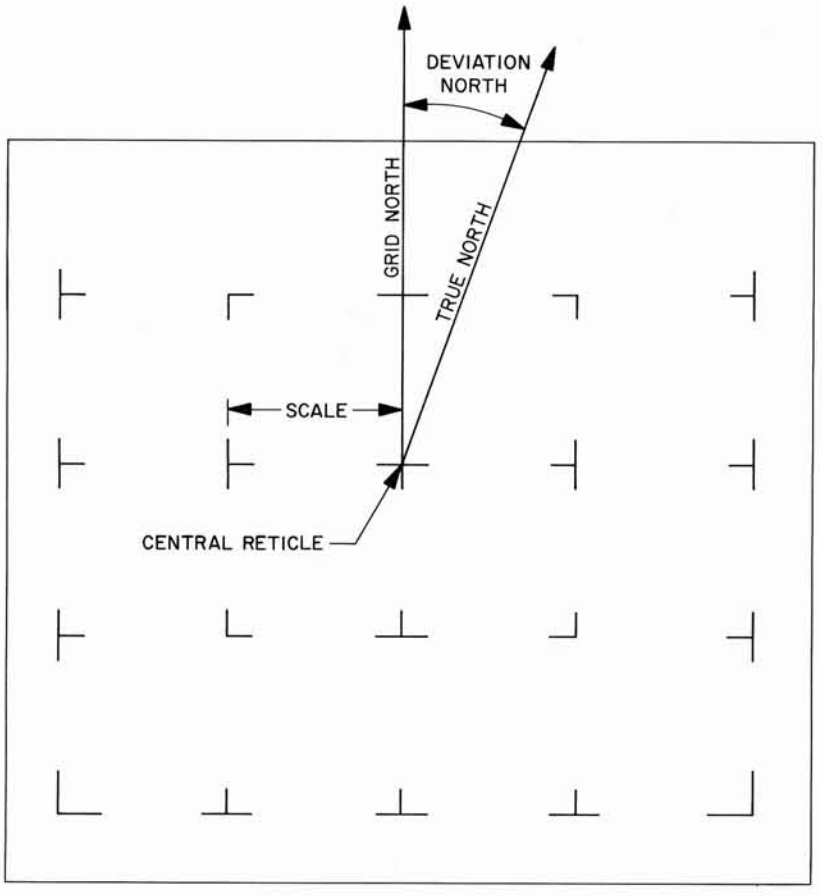

Fig. 9. Definition of central reticle, deviation North, and scale

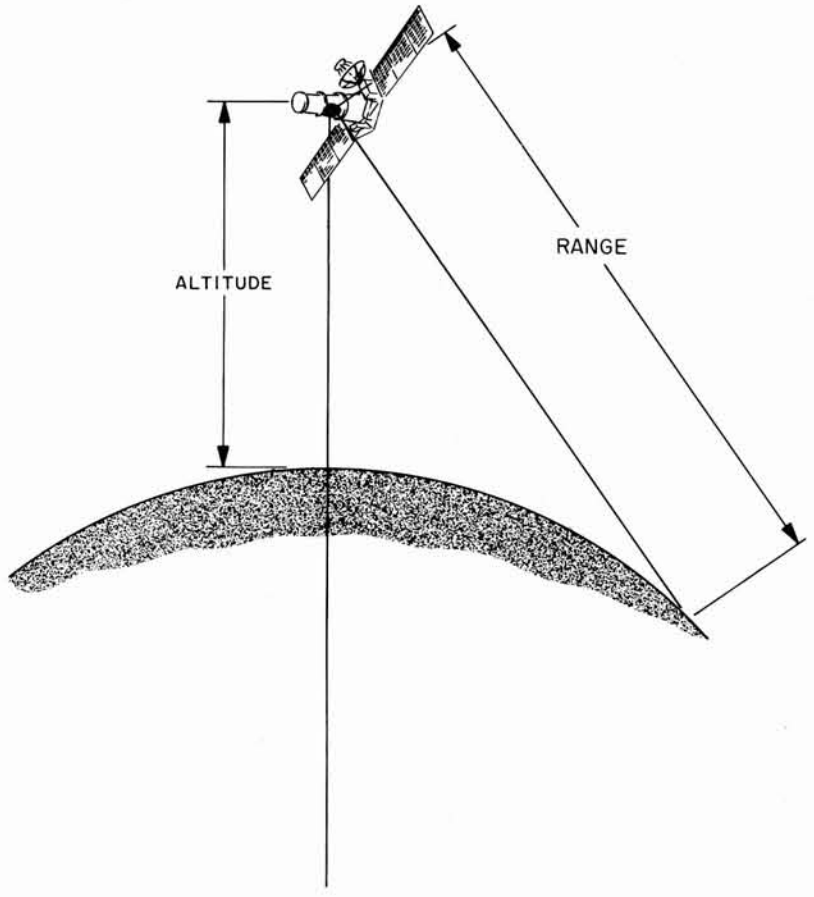

Fig. 10. Altitude and range definition

Table 2. Preliminary table of values*

Photo number	GMT of frame exposure July 31, 1964	Spacecraft			Photograph (central reticle)				Scale,** km	Deviation North,** deg
		Altitude, km	Latitude, deg	Longitude, deg	Latitude, deg	Longitude, deg	Slant range from spacecraft, km	Inclination of surface (normal view, 0 deg)		
1	13:08:52.56	2095.72	−3.29	−35.78	−13.20	−29.96	2158.22	20.7	216.9	5¼
2	13:08:57.68	2086.15	−3.30	−35.75	−13.20	−29.90	2148.67	20.7	216.0	5¼
3	13:09:02.80	2076.58	−3.32	−35.71	−13.19	−29.85	2139.11	20.7	215.2	5¼
4	13:09:07.92	2067.00	−3.34	−35.68	−13.19	−29.80	2129.54	20.7	214.1	5¼
5	13:09:13.04	2057.41	−3.36	−35.64	−13.18	−29.74	2119.96	20.8	213.1	5¼
6	13:09:18.16	2047.82	−3.38	−35.61	−13.18	−29.77	2110.02	20.7	212.1	5¼
7	13:09:23.28	2038.22	−3.39	−35.57	−13.19	−29.80	2100.06	20.7	211.2	5¼
8	13:09:28.40	2028.61	−3.41	−35.53	−13.18	−29.74	2090.46	20.7	210.2	5½
9	13:09:33.52	2019.00	−3.43	−35.50	−13.18	−29.69	2080.85	20.7	209.2	5½
10	13:09:38.64	2009.37	−3.45	−35.46	−13.17	−29.64	2071.23	20.8	208.1	5½
11	13:09:43.76	1999.74	−3.47	−35.42	−13.16	−29.58	2061.61	20.8	207.3	5½
12	13:09:48.88	1990.11	−3.49	−35.39	−13.16	−29.53	2051.97	20.8	206.3	5½
13	13:09:54.00	1980.46	−3.51	−35.35	−13.15	−29.47	2042.33	20.8	205.5	5½
14	13:09:59.12	1970.81	−3.52	−35.31	−13.15	−29.42	2032.69	20.9	204.6	5½
15	13:10:04.24	1961.15	−3.54	−35.28	−13.14	−29.36	2023.03	20.9	203.4	5½
16	13:10:09.36	1951.49	−3.56	−35.24	−13.14	−29.31	2013.36	20.9	202.6	5½
17	13:10:14.48	1941.81	−3.58	−35.20	−13.13	−29.26	2003.69	20.9	201.7	5½
18	13:10:19.60	1932.13	−3.60	−35.16	−13.16	−29.18	1994.50	21.0	200.7	5½
19	13:10:24.72	1922.44	−3.62	−35.13	−13.20	−29.11	1985.28	21.1	200.0	5½
20	13:10:29.84	1912.75	−3.64	−35.09	−13.19	−29.06	1975.58	21.2	198.9	5½
21	13:10:34.96	1903.05	−3.66	−35.05	−13.19	−29.00	1965.87	21.2	198.0	5½

*Values obtained from conic approximation trajectory as derived by D. E. Willingham and W. E. Kirhofer.
**Derived by D. W. G. Arthur.

Table 2. (Cont'd)

Photo number	GMT of frame exposure July 31, 1964	Spacecraft			Photograph (central reticle)				Scale,** km	Deviation North,** deg
		Altitude, km	Latitude, deg	Longitude, deg	Latitude, deg	Longitude, deg	Slant range from spacecraft, km	Inclination of surface (normal view, 0 deg)		
22	13:10:40.08	1893.34	−3.68	−35.01	−13.18	−28.95	1956.15	21.2	196.8	5½
23	13:10:45.20	1883.62	−3.70	−34.97	−13.17	−28.89	1946.42	21.2	195.9	5½
24	13:10:50.32	1873.89	−3.72	−34.93	−13.17	−28.84	1936.69	21.2	194.7	5½
25	13:10:55.44	1864.16	−3.74	−34.89	−13.16	−28.78	1926.94	21.3	193.6	5½
26	13:11:00.56	1854.42	−3.76	−34.85	−13.15	−28.73	1917.19	21.3	192.6	5½
27	13:11:05.68	1844.67	−3.78	−34.81	−13.15	−28.68	1907.42	21.3	191.7	5½
28	13:11:10.80	1834.91	−3.80	−34.77	−13.14	−28.62	1897.65	21.3	190.6	5½
29	13:11:15.92	1825.15	−3.82	−34.73	−13.15	−28.56	1888.06	21.4	189.7	5½
30	13:11:21.04	1815.37	−3.84	−34.69	−13.16	−28.50	1878.47	21.5	188.6	5½
31	13:11:26.16	1805.59	−3.86	−34.65	−13.15	−28.45	1868.67	21.5	187.8	5½
32	13:11:31.28	1795.80	−3.88	−34.61	−13.14	−28.39	1858.86	21.5	186.7	5½
33	13:11:37.40	1786.01	−3.90	−34.57	−13.14	−28.34	1849.04	21.5	185.6	5½
34	13:11:41.52	1776.20	−3.92	−34.53	−13.13	−28.29	1839.21	21.5	184.6	5½
35	13:11:46.64	1766.39	−3.94	−34.49	−13.12	−28.23	1829.38	21.6	183.5	5½
36	13:11:51.76	1756.57	−3.96	−34.45	−13.12	−28.18	1819.53	21.6	182.3	5½
37	13:11:56.88	1746.74	−3.99	−34.40	−13.11	−28.13	1809.67	21.6	181.5	5½
38	13:12:02.00	1736.91	−4.01	−34.36	−13.10	−28.07	1799.81	21.6	180.4	5½
39	13:12:07.12	1727.06	−4.03	−34.32	−13.09	−28.02	1789.93	21.7	179.6	5½
40	13:12:12.24	1717.21	−4.05	−34.28	−13.09	−27.97	1780.05	21.7	178.6	5¾
41	13:12:17.36	1707.35	−4.07	−34.23	−13.09	−27.92	1770.24	21.7	177.4	5¾
42	13:12:22.48	1697.48	−4.09	−34.19	−13.10	−27.87	1760.42	21.8	176.6	5¾
43	13:12:27.60	1687.60	−4.12	−34.15	−13.09	−27.82	1750.50	21.8	175.4	5¾
44	13:12:32.72	1677.71	−4.14	−34.10	−13.08	−27.76	1740.58	21.8	174.5	5¾
45	13:12:37.84	1667.82	−4.16	−34.06	−13.07	−27.71	1730.64	21.8	173.7	5¾
46	13:12:42.96	1657.92	−4.18	−34.01	−13.07	−27.66	1720.69	21.9	172.4	5¾
47	13:12:48.08	1648.00	−4.20	−33.97	−13.06	−27.60	1710.74	21.9	171.6	5¾
48	13:12:53.20	1638.08	−4.23	−33.92	−13.05	−27.55	1700.77	21.9	170.4	5¾
49	13:12:58.32	1628.16	−4.25	−33.88	−13.04	−27.50	1690.79	21.9	169.1	5¾
50	13:13:03.44	1618.22	−4.27	−33.83	−13.03	−27.44	1680.80	22.0	168.3	5¾
51	13:13:08.56	1608.27	−4.30	−33.79	−13.02	−27.39	1670.81	22.0	167.4	5¾
52	13:13:13.68	1598.32	−4.32	−33.74	−13.02	−27.34	1660.80	22.0	166.3	5¾
53	13:13:18.80	1588.35	−4.34	−33.70	−13.03	−27.28	1650.98	22.1	165.4	5¾
54	13:13:23.92	1578.38	−4.37	−33.65	−13.04	−27.23	1641.14	22.1	164.2	5¾
55	13:13:29.04	1568.40	−4.39	−33.60	−13.03	−27.18	1631.10	22.2	163.0	5¾
56	13:13:34.16	1558.41	−4.41	−33.56	−13.02	−27.12	1621.05	22.2	162.0	5¾
57	13:13:39.28	1548.41	−4.44	−33.51	−13.01	−27.07	1610.98	22.2	161.1	5¾
58	13:13:44.40	1538.40	−4.46	−33.46	−13.00	−27.02	1600.91	22.2	160.1	5¾
59	13:13:49.52	1528.38	−4.49	−33.41	−13.00	−26.97	1590.82	22.3	159.3	5¾
60	13:13:54.64	1518.36	−4.51	−33.36	−12.99	−26.91	1580.72	22.3	158.2	5¾
61	13:13:59.76	1508.32	−4.53	−33.31	−12.98	−26.86	1570.61	22.3	157.4	6
62	13:14:04.88	1498.28	−4.56	−33.27	−12.97	−26.81	1560.49	22.3	156.1	6
63	13:14:10.00	1488.22	−4.58	−33.22	−12.96	−26.76	1550.36	22.3	154.8	6
64	13:14:15.12	1478.16	−4.61	−33.17	−12.95	−26.70	1540.21	22.4	154.2	6
65	13:14:20.24	1468.09	−4.63	−33.12	−12.97	−26.61	1530.60	22.5	152.9	6
66	13:14:25.36	1458.01	−4.66	−33.07	−12.99	−26.52	1520.97	22.6	152.1	6
67	13:14:30.48	1447.92	−4.68	−33.02	−12.98	−26.47	1510.78	22.6	151.1	6
68	13:14:35.60	1437.81	−4.71	−32.97	−12.97	−26.42	1500.59	22.7	149.8	6
69	13:14:40.72	1427.70	−4.73	−32.91	−12.96	−26.36	1490.38	22.7	149.0	6
70	13:14:45.84	1417.58	−4.76	−32.86	−12.95	−26.31	1480.16	22.7	148.1	6
71	13:14:50.96	1407.45	−4.79	−32.81	−12.94	−26.26	1469.93	22.7	146.8	6
72	13:14:56.08	1397.32	−4.81	−32.76	−12.93	−26.21	1459.68	22.8	146.0	6
73	13:15:01.20	1387.17	−4.84	−32.71	−12.92	−26.16	1449.43	22.8	144.8	6
74	13:15:06.32	1377.01	−4.87	−32.65	−12.90	−26.10	1439.16	22.8	143.7	6
75	13:15:11.44	1366.84	−4.89	−32.60	−12.89	−26.05	1428.87	22.8	142.9	6
76	13:15:16.56	1356.66	−4.92	−32.55	−12.89	−25.98	1418.78	22.9	141.6	6
77	13:15:21.68	1346.47	−4.95	−32.49	−12.88	−25.91	1408.66	22.9	140.7	6
78	13:15:26.80	1336.27	−4.97	−32.44	−12.87	−25.86	1398.34	23.0	139.7	6
79	13:15:31.92	1326.07	−5.00	−32.38	−12.86	−25.81	1388.00	23.0	138.4	6
80	13:15:37.04	1315.85	−5.03	−32.33	−12.85	−25.76	1377.66	23.0	137.4	6
81	13:15:41.16	1305.62	−5.06	−32.27	−12.84	−25.71	1367.29	23.0	136.5	6

*Values obtained from conic approximation trajectory as derived by D. E. Willingham and W. E. Kirhofer.
**Derived by D. W. G. Arthur.

Table 2. (Cont'd)

Photo number	GMT of frame exposure July 31, 1964	Spacecraft			Photograph (central reticle)				Scale,** km	Deviation North,** deg
		Altitude, km	Latitude, deg	Longitude, deg	Latitude, deg	Longitude, deg	Slant range from spacecraft, km	Inclination of surface (normal view, 0 deg)		
82	13:15:47.28	1295.38	−5.08	−32.22	−12.83	−25.66	1356.92	23.1	135.2	6
83	13:15:52.40	1285.13	−5.11	−32.16	−12.82	−25.61	1346.53	23.1	134.4	6
84	13:15:57.52	1274.87	−5.14	−32.10	−12.81	−25.56	1336.13	23.1	133.3	6
85	13:16:02.64	1264.60	−5.17	−32.05	−12.80	−25.51	1325.71	23.1	132.0	6
86	13:16:07.76	1254.32	−5.20	−31.99	−12.78	−25.46	1315.28	23.2	131.0	6
87	13:16:12.88	1244.03	−5.23	−31.93	−12.77	−25.41	1304.84	23.2	130.0	6
88	13:16:18.00	1233.73	−5.25	−31.87	−12.75	−25.35	1294.33	23.2	128.9	6
89	13:16:23.12	1223.42	−5.28	−31.81	−12.73	−25.29	1283.81	23.2	127.9	6
90	13:16:28.24	1213.09	−5.31	−31.75	−12.72	−25.24	1273.33	23.2	127.0	5¾
91	13:16:33.36	1202.76	−5.34	−31.69	−12.70	−25.19	1262.83	23.3	125.9	5¾
92	13:16:38.48	1192.42	−5.37	−31.63	−12.69	−25.14	1252.32	23.3	124.9	5¾
93	13:16:43.60	1182.06	−5.40	−31.57	−12.68	−25.09	1241.79	23.3	123.8	5¾
94	13:16:48.72	1171.69	−5.43	−31.51	−12.67	−25.04	1231.25	23.3	122.6	5¾
95	13:16:53.84	1161.32	−5.46	−31.45	−12.66	−25.00	1220.69	23.4	121.8	5¾
96	13:16:58.96	1150.93	−5.49	−31.39	−12.64	−24.95	1210.12	23.4	120.7	5¾
97	13:17:04.08	1140.53	−5.52	−31.33	−12.63	−24.90	1199.53	23.4	119.4	5½
98	13:17:09.20	1130.12	−5.56	−31.26	−12.62	−24.85	1188.93	23.4	118.5	5½
99	13:17:14.32	1119.70	−5.59	−31.20	−12.61	−24.80	1178.31	23.5	117.3	5½
100	13:17:19.44	1109.26	−5.62	−31.14	−12.58	−24.77	1167.42	23.4	116.0	5½
101	13:17:24.56	1098.82	−5.65	−31.07	−12.56	−24.74	1156.51	23.4	115.2	5½
102	13:17:29.68	1088.36	−5.68	−31.01	−12.54	−24.69	1145.85	23.4	114.3	5½
103	13:17:34.80	1077.90	−5.71	−30.94	−12.53	−24.64	1135.17	23.4	112.8	5½
104	13:17:39.92	1067.42	−5.75	−30.88	−12.52	−24.59	1124.48	23.5	111.9	5½
105	13:17:45.04	1056.93	−5.78	−30.81	−12.50	−24.54	1113.77	23.5	110.9	5½
106	13:17:50.16	1046.42	−5.81	−30.75	−12.49	−24.49	1103.05	23.5	109.6	5½
107	13:17:55.28	1035.91	−5.85	−30.68	−12.48	−24.44	1092.31	23.5	108.5	5½
108	13:18:00.40	1025.38	−5.88	−30.61	−12.47	−24.39	1081.55	23.6	107.5	5½
109	13:18:05.52	1014.85	−5.91	−30.54	−12.45	−24.34	1070.77	23.6	106.2	5½
110	13:18:10.64	1004.30	−5.95	−30.47	−12.44	−24.29	1059.98	23.6	105.1	5¼
111	13:18:15.76	993.73	−5.98	−30.40	−12.43	−24.25	1049.18	23.6	104.1	5¼
112	13:18:20.88	983.16	−6.01	−30.33	−12.40	−24.22	1038.03	23.6	103.0	5¼
113	13:18:26.00	972.57	−6.05	−30.26	−12.37	−24.20	1026.87	23.6	101.9	5¼
114	13:18:31.12	961.97	−6.08	−30.19	−12.36	−24.15	1016.02	23.6	100.9	5¼
115	13:18:36.24	951.36	−6.12	−30.12	−12.35	−24.10	1005.15	23.6	99.8	5
116	13:18:41.36	940.74	−6.15	−30.05	−12.33	−24.05	994.26	23.6	98.5	5
117	13:18:46.48	930.10	−6.19	−29.98	−12.32	−24.00	983.35	23.6	97.4	5
118	13:18:51.60	919.45	−6.23	−29.90	−12.30	−23.96	972.42	23.7	96.4	5
119	13:18:56.72	908.79	−6.26	−29.83	−12.29	−23.91	961.48	23.7	95.3	5
120	13:19:01.84	898.12	−6.30	−29.75	−12.28	−23.86	950.52	23.7	94.1	5
121	13:19:06.96	887.43	−6.34	−29.68	−12.26	−23.81	939.54	23.7	93.2	5
122	13:19:12.08	876.73	−6.37	−29.60	−12.25	−23.76	928.54	23.8	91.9	5
123	13:19:17.20	866.02	−6.41	−29.53	−12.23	−23.73	917.40	23.8	90.6	5
124	13:19:22.32	855.29	−6.45	−29.45	−12.21	−23.69	906.24	23.8	89.8	5
125	13:19:27.44	844.55	−6.49	−29.37	−12.19	−23.64	895.18	23.8	88.5	5
126	13:19:32.56	833.80	−6.52	−29.29	−12.18	−23.59	884.11	23.8	87.4	5
127	13:19:37.68	823.03	−6.56	−29.21	−12.16	−23.54	873.02	23.8	86.4	5
128	13:19:42.80	812.25	−6.60	−29.13	−12.15	−23.50	861.90	23.8	85.3	5
129	13:19:47.92	801.46	−6.64	−29.05	−12.13	−23.45	850.77	23.9	84.0	5
130	13:19:53.04	790.65	−6.68	−28.97	−12.12	−23.40	839.62	23.9	83.0	5
131	13:19:58.16	779.83	−6.72	−28.89	−12.10	−23.36	828.45	23.9	82.1	5
132	13:20:03.28	769.00	−6.76	−28.81	−12.09	−23.31	817.25	23.9	80.8	5
133	13:20:08.40	758.15	−6.80	−28.73	−12.07	−23.26	806.04	24.0	79.8	5¼
134	13:20:13.52	747.29	−6.84	−28.64	−12.05	−23.22	794.80	24.0	78.7	5¼
135	13:20:18.64	736.41	−6.88	−28.56	−12.02	−23.17	783.42	24.0	77.4	5¼
136	13:20:23.76	725.52	−6.93	−28.47	−11.99	−23.12	772.01	24.0	76.6	5½
137	13:20:28.88	714.61	−6.97	−28.38	−11.98	−23.08	760.71	24.0	75.5	5½
138	13:20:34.00	703.70	−7.01	−28.30	−11.96	−23.03	749.39	24.0	74.0	5½
139	13:20:39.12	692.76	−7.05	−28.21	−11.94	−22.99	738.06	24.0	73.2	5½
140	13:20:44.24	681.81	−7.10	−28.12	−11.93	−22.94	726.69	24.0	72.1	5¾
141	13:20:49.36	670.85	−7.14	−28.03	−11.91	−22.90	715.31	24.1	70.8	5¾

*Values obtained from conic approximation trajectory as derived by D. E. Willingham and W. E. Kirhofer.
**Derived by D. W. G. Arthur.

Table 2. (Cont'd)

Photo number	GMT of frame exposure July 31, 1964	Spacecraft			Photograph (central reticle)				Scale,** km	Deviation North,** deg
		Altitude, km	Latitude, deg	Longitude, deg	Latitude, deg	Longitude, deg	Slant range from spacecraft, km	Inclination of surface (normal view, 0 deg)		
142	13:20:54.48	659.87	−7.18	−27.94	−11.90	−22.85	703.90	24.1	69.8	6
143	13:20:59.60	648.88	−7.23	−27.85	−11.88	−22.81	692.47	24.1	68.7	6
144	13:21:04.72	637.87	−7.27	−27.76	−11.86	−22.76	681.02	24.1	67.6	6¼
145	13:21:09.84	626.85	−7.32	−27.66	−11.84	−22.72	669.54	24.2	66.3	6¼
146	13:21:14.96	615.81	−7.36	−27.57	−11.83	−22.67	658.05	24.2	65.0	6½
147	13:21:20.08	604.76	−7.41	−27.47	−11.80	−22.63	646.48	24.2	64.1	6½
148	13:21:25.20	593.69	−7.45	−27.38	−11.78	−22.58	634.90	24.2	62.8	6½
149	13:21:30.32	582.60	−7.50	−27.28	−11.76	−22.54	623.33	24.2	61.6	6½
150	13:21:35.44	571.50	−7.55	−27.18	−11.75	−22.50	611.73	24.2	60.7	6½
151	13:21:40.56	560.39	−7.60	−27.08	−11.73	−22.45	600.11	24.3	59.5	6¾
152	13:21:45.68	549.26	−7.64	−26.98	−11.71	−22.41	588.46	24.3	58.1	6¾
153	13:21:50.80	538.11	−7.69	−26.88	−11.69	−22.37	576.79	24.3	57.1	6¾
154	13:21:55.92	526.95	−7.74	−26.78	−11.67	−22.32	565.10	24.3	56.0	6¾
155	13:22:01.04	515.77	−7.79	−26.68	−11.66	−22.28	553.37	24.3	54.7	6¾
156	13:22:06.16	504.57	−7.84	−26.57	−11.64	−22.24	541.62	24.4	53.3	6¾
157	13:22:11.28	493.36	−7.89	−26.47	−11.62	−22.20	529.85	24.4	52.3	6¾
158	13:22:16.40	482.13	−7.94	−26.36	−11.60	−22.16	518.06	24.4	51.3	6¾
159	13:22:21.52	470.89	−7.99	−26.26	−11.59	−22.11	506.25	24.4	49.9	6¾
160	13:22:26.64	459.62	−8.04	−26.15	−11.57	−22.07	494.39	24.4	48.6	6¾
161	13:22:31.76	448.34	−8.10	−26.04	−11.55	−22.03	482.51	24.5	47.6	6¾
162	13:22:36.88	437.05	−8.15	−25.93	−11.53	−21.99	470.59	24.5	46.5	6¾
163	13:22:42.00	425.73	−8.20	−25.82	−11.51	−21.95	458.65	24.5	45.1	6¾
164	13:22:47.12	414.40	−8.26	−25.70	−11.48	−21.91	446.68	24.5	43.9	6¾
165	13:22:52.24	403.06	−8.31	−25.59	−11.46	−21.87	434.67	24.5	42.8	6¾
166	13:22:57.36	391.69	−8.36	−25.47	−11.44	−21.83	422.64	24.5	41.7	6¾
167	13:23:02.48	380.31	−8.42	−25.36	−11.42	−21.79	410.58	24.6	40.2	6¾
168	13:23:07.60	368.91	−8.48	−25.24	−11.40	−21.75	398.49	24.6	39.1	7
169	13:23:12.72	357.49	−8.53	−25.12	−11.38	−21.71	386.37	24.6	38.1	7
170	13:23:17.84	346.05	−8.59	−25.00	−11.36	−21.67	374.26	24.6	36.9	7
171	13:23:22.96	334.59	−8.65	−24.88	−11.34	−21.63	362.12	24.7	35.4	7
172	13:23:28.08	323.12	−8.71	−24.75	−11.32	−21.59	349.90	24.7	34.3	7
173	13:23:33.20	311.63	−8.76	−24.63	−11.30	−21.55	337.65	24.7	33.2	7
174	13:23:38.32	300.12	−8.82	−24.50	−11.27	−21.51	325.36	24.7	32.0	7
175	13:23:43.44	288.59	−8.88	−24.37	−11.25	−21.48	313.05	24.7	30.7	7
176	13:23:48.56	277.04	−8.95	−24.24	−11.23	−21.44	300.70	24.7	29.5	7
177	13:23:53.68	265.47	−9.01	−24.11	−11.20	−21.40	288.32	24.7	28.3	7
178	13:23:58.80	253.89	−9.07	−23.98	−11.18	−21.37	275.90	24.8	27.2	7
179	13:24:03.92	242.28	−9.13	−23.84	−11.15	−21.33	263.45	24.8	25.8	7
180	13:24:09.04	230.65	−9.20	−23.71	−11.13	−21.30	250.96	24.8	24.5	7
181	13:24:14.16	219.01	−9.26	−23.57	−11.10	−21.26	238.44	24.8	23.3	7
182	13:24:19.28	207.34	−9.32	−23.43	−11.08	−21.23	225.90	24.8	22.0	7
183	13:24:24.40	195.66	−9.39	−23.29	−11.06	−21.19	213.32	24.8	20.6	7¼
184	13:24:29.52	183.95	−9.46	−23.15	−11.03	−21.16	200.69	24.9	19.3	7¼
185	13:24:34.64	172.23	−9.52	−23.00	−11.01	−21.12	188.02	24.9	18.0	7¼
186	13:24:39.76	160.48	−9.59	−22.86	−10.98	−21.09	175.31	24.9	16.9	7¼
187	13:24:44.88	148.72	−9.66	−22.71	−10.95	−21.06	162.57	24.9	15.60	7¼
188	13:24:50.00	136.93	−9.73	−22.56	−10.93	−21.02	149.78	24.9	14.40	7¼
189	13:24:55.12	125.12	−9.80	−22.41	−10.90	−20.99	136.96	24.9	13.15	7¼
190	13:25:00.24	113.29	−9.87	−22.25	−10.87	−20.96	124.10	24.9	11.91	7¼
191	13:25:05.36	101.44	−9.94	−22.09	−10.84	−20.93	111.19	24.9	10.65	7¼
192	13:25:10.48	89.57	−10.02	−21.94	−10.81	−20.90	98.25	24.9	9.40	7¼
193	13:25:15.60	77.68	−10.09	−21.78	−10.79	−20.86	85.26	24.9	8.15	7¼
194	13:25:20.72	65.76	−10.16	−21.61	−10.76	−20.83	72.26	25.0	6.89	7¼
195	13:25:25.84	53.82	−10.24	−21.45	−10.73	−20.80	59.19	25.0	5.65	7¼
196	13:25:30.96	41.86	−10.32	−21.28	−10.70	−20.78	46.07	25.0	4.39	7¼
197	13:25:36.08	29.88	−10.39	−21.11	−10.67	−20.75	32.91	25.0	3.14	7¼
198	13:25:41.20	17.88	−10.47	−20.94	−10.64	−20.72	19.71	25.0	1.92	7¼
199	13:25:46.32	5.85	−10.55	−20.76	−10.60	−20.69	6.46	25.0	0.647	7¼
IMPACT	13:25:48.82	0.	−10.59	−20.68						

*Values obtained from conic approximation trajectory as derived by D. E. Willingham and W. E. Kirhofer.
**Derived by D. W. G. Arthur.

REFERENCES

1. Rindfleisch, T. C., and Willingham, D. E., *Figure of Merit as a Measure of Picture Resolution,* Technical Report No. 32-666, Jet Propulsion Laboratory, Pasadena, California (to be published).
2. Kirhofer, W. E., *Television Constraints and Digital Computer Program,* Technical Report No. 32-667, Jet Propulsion Laboratory, Pasadena, California (to be published).
3. Sytinskaya, N. N., and Sharonov, V. V., "Study of the Reflecting Power of the Moon's Surface," *Uchenye Zapiski Lgu,* No. 153 (1952), p. 114. (Translated by Space Technology Laboratories, Inc., Los Angeles, California, as STL-TR-61-5110-23, May 1961.)
4. Willingham, D. E., *The Lunar Reflectivity Model for Ranger Block III Analysis,* Technical Report No. 32-664, Jet Propulsion Laboratory, Pasadena, California (to be published).
5. Smith, G. M., and Willingham, D. E., *Ranger Photometric Calibration,* Technical Report No. 32-665, Jet Propulsion Laboratory, Pasadena, California (to be published).